

## Thick target neutron yield from 145 MeV $^{19}\text{F}+^{27}\text{Al}$ system



Sunil C. <sup>a,\*</sup>, T. Bandyopadhyay <sup>a</sup>, M. Nandy <sup>b</sup>, Vitisha Suman <sup>a</sup>, S. Paul <sup>a</sup>, V. Nanal <sup>c</sup>,  
R.G. Pillay <sup>c</sup>, P.K. Sarkar <sup>a</sup>

<sup>a</sup> Accelerator Radiation Safety Section, Health Physics Division, BARC, Mumbai 400085, India

<sup>b</sup> Saha Institute of Nuclear Physics, Kolkata, India

<sup>c</sup> DNAP, TIFR, Mumbai 400005, India

### ARTICLE INFO

#### Article history:

Received 15 March 2013

Received in revised form

13 April 2013

Accepted 14 April 2013

Available online 24 April 2013

#### Keywords:

Thick Target Neutron Yield

Heavy ion reaction

Neutron time of flight

PACE

### ABSTRACT

The double differential neutron energy distribution has been measured for the  $^{19}\text{F}+^{27}\text{Al}$  system at 145 MeV projectile energy. The time of flight technique was used to measure the energy while pulse shape discrimination has been used to separate the neutrons from photons. The results are compared with the statistical nuclear reaction model codes PACE and EMPIRE. The PACE code appears to predict the slope and the end point energy of the experimental spectra fairly well but over predicts the values. The slope obtained from the EMPIRE calculations appears to be harder while the values being closer to the experimental results. The yield from the Hauser–Feshbach based compound nucleus model calculations agree reasonably well with the experimental results at the backward angles but not in the forward directions. The energy integrated angular distribution from 145 MeV projectiles show an enhanced emission in the forward angles compared to the similar results from 110 MeV projectiles. This analysis suggests some contribution from the pre-equilibrium emissions from the system at the higher projectile energy.

© 2013 Elsevier B.V. All rights reserved.

### 1. Introduction

Energy–angle distribution of the thick target neutron yield (TTNY) is the fundamental measurable quantity required for all radiation protection calculations in positive ion accelerators [1]. This is because neutrons constitute the major component of prompt radiation produced during beam loss that needs to be shielded and measured for personnel, equipment and environmental protection against radiation hazard in such accelerator facilities. Estimation of neutron dose equivalent requires information on the energy distribution of neutrons since the fluence to dose conversion coefficient is a strong function of neutron energy. The energy spectra can be converted to ambient and personal dose equivalents by folding with the appropriate fluence to dose conversion coefficients given by International Commission of Radiological Protection (ICRP) [2]. Since the spectra remain invariant for a particular system (projectile–target–beam energy combination) under study, any change in the conversion coefficients can be readily incorporated to derive the new dose equivalent quantities. Such data are also important from the point of view of estimating the probability of latent cancer induction by the secondary particles produced during heavy ion therapy [3,4]. The primary ion slows down in the tissue before being absorbed,

emitting neutrons and other secondary particles in the process which in turn interact with the healthy tissue surrounding a tumor. A beam loss condition, either in an accelerator component or in the tissue, is simulated by a thick target since in both the cases the projectile is completely stopped. This is the worst case scenario as the secondary particle yield will be at its maximum and is the starting point for all radiation protection calculations. The inclusive neutron yield is thus a sum of all the emissions for projectile energies starting from the initial beam energy to either the Coulomb barrier or the reaction threshold [5]. Very often, such data are obtained by experiments and by calculations using nuclear reaction or Monte Carlo codes. Since it is not possible to measure the yield from every projectile target combination, the systematics of the emission need to be studied with respect to the projectile–target parameters either with an empirical model or by nuclear reaction model calculations. Experimental data are required for fine tuning of the input parameters in statistical nuclear reaction model codes and for the formulation, comparison and validation of empirical techniques.

The neutron yield measurements have been few and far between for projectile energies less than 10 MeV/amu. Only a few measurements in this energy region have been reported in the literature [6–10]. Moreover, at incident energies of about 7 MeV/amu, some amount of pre-equilibrium emissions have been reported for a heavier composite system [8] and it would be interesting to study the double differential neutron yield from a lower compound nuclear mass for such an evidence.

\* Corresponding author. Tel.: +91 22 25592012; fax: +91 22 25505313.  
E-mail address: [sunilc@barc.gov.in](mailto:sunilc@barc.gov.in) (S. C.).

In this work, the neutron energy distributions at  $0^\circ$ ,  $30^\circ$ ,  $60^\circ$ ,  $90^\circ$  and  $120^\circ$  with respect to the beam direction have been measured from 145 MeV  $^{19}\text{F}$  projectiles incident on a thick Al target using the time of flight (ToF) technique. The experimental results are compared with calculations of the PACE-2 [11] and the EMPIRE-2.18 [12] statistical nuclear reaction model codes.

## 2. Experiment

The experiment was carried out at the linac extension of the BARC-TIFR Pelletron-Linac Accelerator Facility, Mumbai, India. Five EJ301 liquid (recoil proton) scintillators of size  $5\text{ cm} \times 5\text{ cm}$  (Scionix Holland make) were kept at 1.5 m from the target at  $0^\circ$ ,  $30^\circ$ ,  $60^\circ$ ,  $90^\circ$  and  $120^\circ$  with respect to the beam direction. The Al target was made in the shape of a hemisphere of 3 mm thickness and 40 mm diameter to reduce attenuation of the emerging neutrons. At 145 MeV,  $^{19}\text{F}$  ions have a range of 0.11 mm in Al [13]. Pulse shape discrimination by the zero cross over method was used to separate neutrons from gamma photons while ToF technique was used to measure the neutron energy. The experimental arrangement is shown in Fig. 1. Since the measurements were inclusive in nature, background contribution from scattered neutrons was measured separately using a shadow bar consisting of 30 cm iron followed by 30 cm of high density polyethylene (HDPE). The shadow bar stops the direct neutrons thereby enabling measurement of only the scattered neutrons. The background spectra thus obtained were subtracted from the total spectra measured without the shadow bar to get the net counts due to the direct neutrons only. The total yield was measured at 5 angles simultaneously, while the shadow bar runs were carried out one angle at a time. The detector to detector in-scattering was assumed to be negligible. The electronic set-up used in the experiment is shown schematically in Fig. 2. The anode output of the PMT (photo multiplier tube) was used as the input to a CFD (constant fraction discriminator, Ortec 935) and in parallel to a PSD (pulse shape discriminator, FAST ComTec 2160A). The CFD and PSD outputs provide the start and the

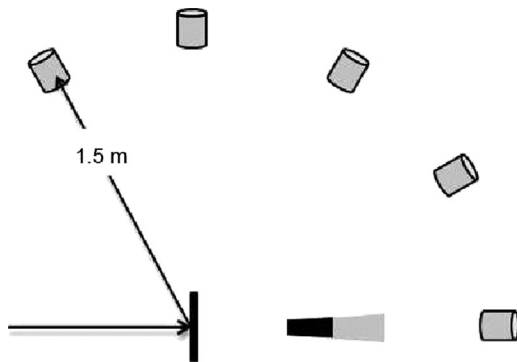


Fig. 1. Experimental arrangement with the shadow bar used for the background subtraction.

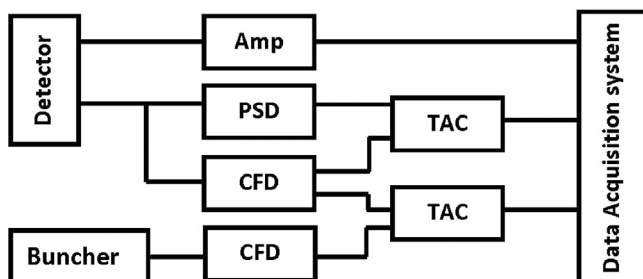


Fig. 2. A simplified block diagram of the electronics setup used involving one detector.

stop signals for a TAC (time to amplitude converter, Ortec 567) whose output is proportional to the time difference. This helps distinguish the neutron pulses from the gamma pulses due to the difference in their decay times. The direct current beam was pulsed using a buncher with the pulses separated by 100 ns. The Gaussian time spread of the beam had a full width at half maximum (FWHM) of 0.75 ns. The buncher signal obtained through a second CFD and the detector signal from the first CFD were used in another TAC to derive the flight time information. The dynode output of the PMT was given to a spectroscopic amplifier (CAEN N968) for the energy signal. One detector therefore gives three parameters ( $n$ - $\gamma$  discrimination, ToF and the energy) and the 15 signals from the five detectors were acquired by an ADC in the list mode format for offline analysis. An OR logic of the CFD signals from all the five detectors was used to generate a master gate for the CAMAC based data acquisition system. Fig. 2 shows a simplified block diagram of the electronics setup involving just one detector. Figs. 3 and 4 show the TAC outputs of the PSD and ToF respectively. Fig. 5 shows a two-dimensional plot with these two parameters on the abscissa (ToF) and ordinate (PSD). The  $n$ - $\gamma$  separation which is evident in Figs. 3 and 4 is accentuated in the contour plot (Fig. 5). In an offline analysis, software gates can be drawn easily on such a plot to identify the neutron events alone. The information is used to extract the ToF information from the list mode data on an event by event basis. A precision beam current monitor (Ortec 439) was used to measure the integral charge incident on the target. The counts are binned in 0.5 MeV width energy intervals, corrected for the energy dependent efficiency (Fig. 6), the solid angle and the total charge incident, to

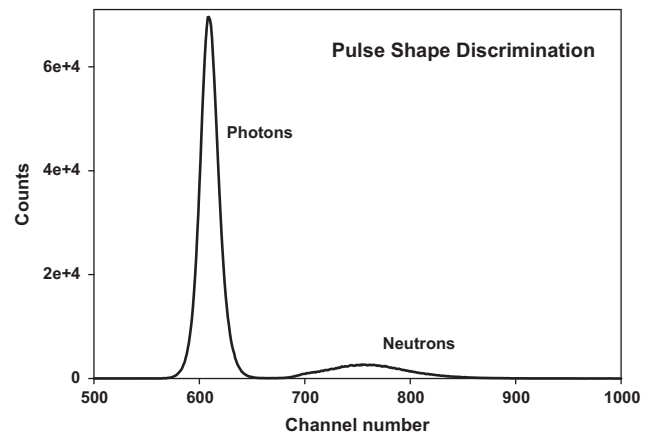


Fig. 3. Measured one-dimensional pulse shape discrimination spectrum for neutrons and photons.

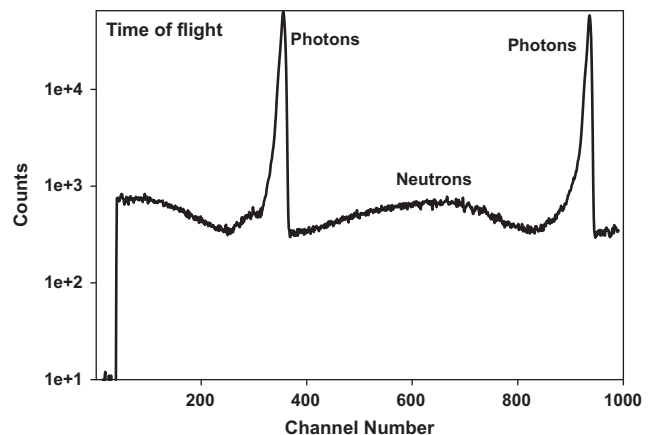


Fig. 4. Measured one-dimensional ToF spectra showing the neutrons and photons. Two bursts of the beam are seen in the TAC region.

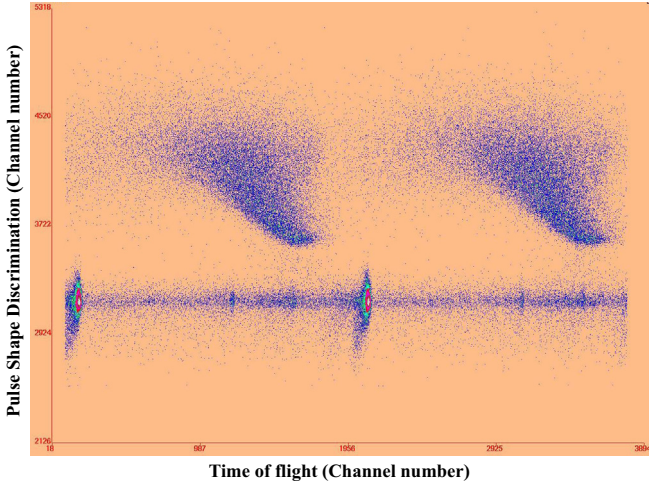


Fig. 5. 2D contour plot of PSD and TOF spectra from the present experiment showing n- $\gamma$  separation. Two bursts of the beam are seen in the TAC region.

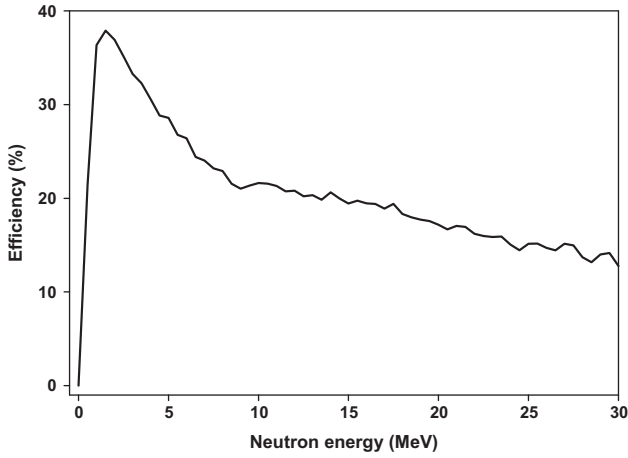


Fig. 6. An efficiency plot for the EJ301 detector.

obtain the neutron spectra in units of  $\text{MeV}^{-1} \text{sr}^{-1} \text{ion}^{-1}$ . The efficiency was obtained by the Monte Carlo calculations [14] and is assumed to be the same for all the detectors.

### 3. Uncertainties in the results

#### 3.1. Energy uncertainty

Kurosawa et al. [15] have outlined the sources of error for measurement of energy spectra by the ToF technique. The relative energy resolution is given by

$$\frac{\Delta E}{E} = \gamma(\gamma + 1) \left( \frac{\Delta t}{t} \right) \quad (1)$$

where

$$\gamma = 1 + \frac{E}{Mc^2} \quad (2)$$

Here  $E$  is the neutron kinetic energy,  $M$  is its rest mass,  $\Delta t$  the overall time resolution and  $t$  the neutron flight time. The factors contributing to the time resolution are the intrinsic time resolution of the detector, the time spread in the prompt gamma peak which is directly proportional to the beam bunch spread, beam energy spread, the time difference in neutron production in the thick target and the difference in time taken for the neutron to travel the

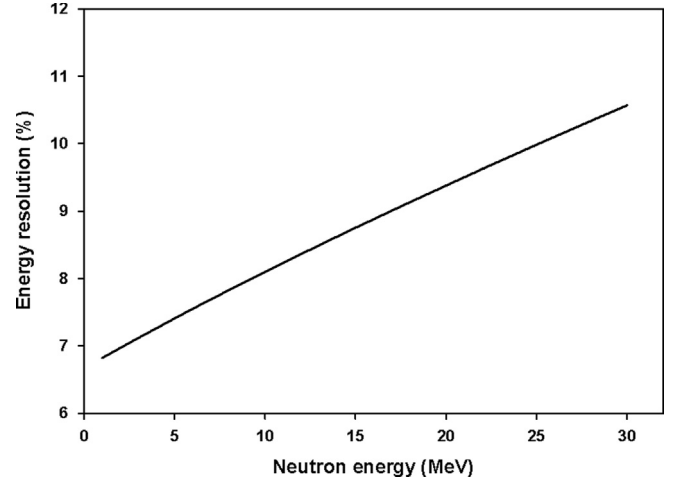


Fig. 7. The percentage energy resolution as a function of the neutron energy for the present experimental results.

finite thickness of the detector. When factors like time dispersions due to beam energy spread and finite thickness of the target are ignored as negligible, the major contributing factors are the time spread of the beam pulse and the intrinsic time resolution of the neutron detector;

Thus  $\Delta t$  can be expressed as

$$\Delta t = \left( (\Delta \tau)^2 + \left( \frac{\Delta x}{v} \right)^2 \right)^{1/2} \quad (3)$$

where  $\Delta \tau$  is the time spread due to the beam pulse width,  $\Delta x$  is the thickness of the detector and  $v$  is the velocity of the incident neutron. The results obtained using Eq. (1) expressed as percentage for the present experimental data are shown in Fig. 7.

#### 3.2. Statistical and other uncertainties

The statistical uncertainty arises from the counts in the energy bin and the process of subtracting the room-scattered background. These scattered background counts were determined by measurements at the same angles after placing the shadow bar shields as described before. The room-scattered contribution was found to be about 1% in the forward direction ( $0^\circ$ – $30^\circ$ ) and about 5% at the backward angles ( $90^\circ$  and  $120^\circ$ ). The propagated errors from these are shown as the vertical error bars in the results. The uncertainty in the solid angle is estimated to be less than 2% while for the precision beam current monitor, it is less than 1%. The detection efficiencies calculated using the Monte Carlo technique has about 2% uncertainty in it.

### 4. Statistical model calculations

In order to analyze and understand the reaction mechanism involved, double differential thick target neutron yield (TTNY) have been calculated using the statistical nuclear reaction model codes PACE2 and EMPIRE 2.18 and compared with the measured data.

The Projection Angular-momentum Coupled Evaporation (PACE) code uses the Monte Carlo technique for simulation of the de-excitation process of the compound nucleus through various available decay channels. The code tracks particles based on the statistical model with a complete account of the angular momentum including  $\gamma$ -emissions at all stages of evaporation. In the present study, de-excitation of the compound nucleus was calculated using the Hauser-Feshbach formalism and the transmission coefficients for emission of

the light particles were calculated with the default optical model potentials. Fusion cross-section for formation of the compound nucleus was calculated using the Bass model [16] and the decay to the various channels were estimated according to their respective probabilities after normalizing the initial spin distribution to unity. Level density of the compound and the residual nuclei was calculated using the Fermi gas model with the level density parameter 'a' set to  $A/7 \text{ MeV}^{-1}$  where A is the mass number of the nucleus.

Neutron energy distribution was also calculated from the EMPIRE code using EMPIRE specific level density option which is recommended in the code as the best option for heavy ion induced reactions. The fusion cross section is calculated internally using the simplified coupled channel approach. This approach results in fusion cross sections close to the experimental data up to about 80 MeV, but at higher energies the calculations over predict the experimental as well as the Bass model predictions. From this energy spectrum, angular distribution is calculated considering isotropic distribution in the CM (center of mass) frame and then converting it to the laboratory frame.

The emission cross sections from these codes were evaluated separately starting from the initial projectile energy upto about the Coulomb barrier. The thick target yield is a sum of emissions from the continuously degrading projectile energy. The slowing down is considered in small discrete steps and the thick target is divided into a number of thin slabs such that the projectile loses a specified energy (5 MeV in this work) in each slab. SRIM2008 [13] code was used to calculate the energy loss at every step. The projectile is assumed to interact with all target nuclei in its path within this thin slab with an average energy and the corresponding emission cross sections are calculated. These emitted spectra from all of the slabs are summed up to give the thick target yield, with a correction for the fraction of the projectiles that are transmitted to the next slab as a function of the fusion cross section. More details can be found in [7].

## 5. Results and discussions

The results of experimental measurements of the double differential TNY for 145 MeV  $^{19}\text{F}+^{27}\text{Al}$  system and their comparison with the calculated results using the PACE and the EMPIRE codes are shown in Fig. 8 where, the experimental results are shown as symbols, the PACE results as solid lines and the EMPIRE results as broken lines. The statistical uncertainties in the experiment are shown as vertical error bars. The measured neutron spectra at all angles have a lower energy cut-off of 1 MeV determined by the flight

path and the threshold settings. The measured yield is plotted up to the energy where no statistical oscillations are observed. The data extend upto about 30 MeV in the forward directions and this maximum neutron emission energy gradually decreases at backward angles. The peak in the energy distribution occurs at about 4 MeV at  $0^\circ$  and shifts to about 3 MeV at  $30^\circ$  and  $60^\circ$  and to about 1.5 MeV at the backward angles.

In the double differential neutron yield obtained from the PACE code, the peak energy is seen to be slightly higher than what is observed in the measured spectra at forward angles while they approximately match at backward angles. The highest neutron energy observed in the experimental data appears to be higher by a few MeV at  $0^\circ$  and  $30^\circ$  compared to the results from the PACE code while it is lower at the backward angles. The slope of the calculated spectra approximately agrees well with the experimental data at all angles of emission except at the highest energies in the forward direction, where some difference is observed. The double differential yield obtained from the PACE code is higher by 1.5 to 3 times in the forward angles at all energies except in the 1–2 MeV region, but tends to approximately match with the experimental data at higher energies at larger emission angles. The highest neutron energy predicted by the PACE code decreases with increasing angle of emission.

The peak energies of the spectra obtained by the EMPIRE code calculations are lower than that obtained by the experiment and the PACE calculations at  $0^\circ$  and at  $30^\circ$  while it is higher at all other angles. The double differential yield approximately agrees with the experimental results in the low energy region at all angles except for the extreme forward angle ( $0^\circ$ ) where it under-predicts the measured values. As the neutron energy increases EMPIRE gives a larger value of neutron yield compared to the measured results at  $30^\circ$ ,  $60^\circ$ ,  $90^\circ$  and  $120^\circ$ . For neutron energies above 15 MeV, EMPIRE predicts the measured yield well at  $0^\circ$ . The slope slopes of the spectra calculated by the EMPIRE code are not in agreement with either the experimental data or with the PACE results.

In Fig. 9, the present results are compared with the TNY obtained for 110 MeV  $^{19}\text{F}+^{27}\text{Al}$  system reported in our earlier work [7]. The yield from 145 MeV projectiles is found to be about 2–4 times higher than that obtained from 110 MeV projectiles. The ratio is higher in the forward angles and lower at the backward angles. The increase is approximately the same for all angles except at  $60^\circ$  where it is seen to be lower, possibly due to the variation in the efficiency used for the detector used during the present experiment compared to the values obtained by the Monte Carlo calculation. While only one detector was used to carry out the measurements with 110 MeV projectiles, 5 separate detectors were used with 145 MeV projectiles.

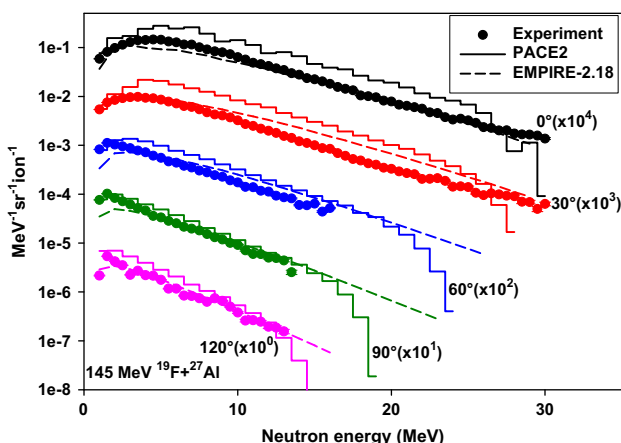


Fig. 8. The Double differential neutron yield obtained from the experiment and from the nuclear reaction model calculations.

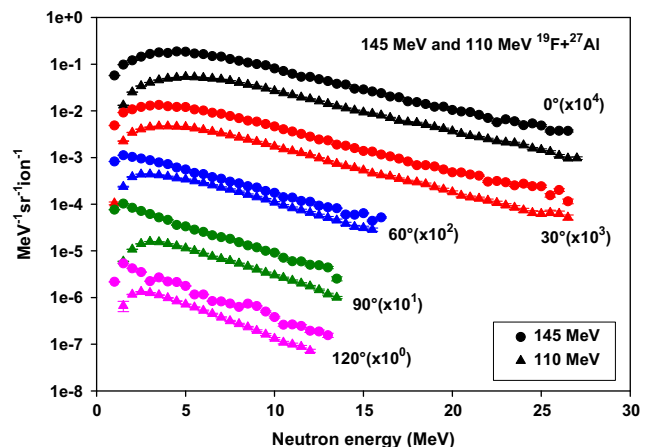
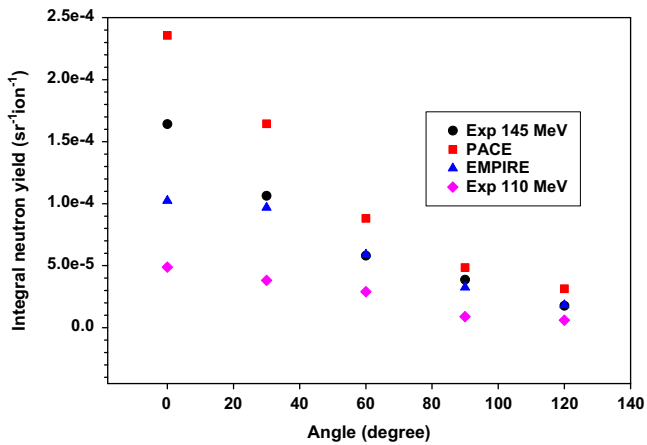


Fig. 9. Comparison of the neutron energy spectra from 110 and 145 MeV  $^{19}\text{F}+^{27}\text{Al}$  systems.



**Fig. 10.** Energy integrated neutron yield as a function of the emission angle obtained from the experiments and the nuclear reaction model calculations.

The energy integrated angular distribution of the neutron yield is shown in Fig. 10. The calculated yield obtained from the PACE code is about 1.5 times higher at  $0^\circ$ – $90^\circ$  and 2 times higher at  $120^\circ$  compared to the experimental results. The results from the EMPIRE code are 60% of the experimental value at  $0^\circ$  and 80–100% at all other angles. For the same target-projectile system, the neutron yields from 145 MeV projectiles are 2–4 times higher compared to that from 110 MeV projectiles.

The present experimental data indicate that the highest neutron energy emitted at forward angles is higher than what is predicted by the Hauser–Feshbach model of emission from a compound nucleus. Such compound nuclear emissions are able to explain the double differential yield at  $90^\circ$  and  $120^\circ$  satisfactorily but not at  $0^\circ$  and  $30^\circ$ . Also, the energy integrated yield for the higher projectile energy shows an appreciable enhancement in the forward direction compared to similar results obtained at a lower projectile energy. These results suggest that there could be some pre-equilibrium neutron emission from the 145 MeV  $^{19}\text{F}+^{27}\text{Al}$  system though not very conclusively significant.

## 6. Summary and conclusions

The thick target neutron yield from 145 MeV  $^{19}\text{F}$  projectiles is measured using time of flight technique and is compared with

statistical model calculations. In the PACE calculations Fermi gas level density with the 'a' parameter as  $A/7$  is used while calculations using the EMPIRE code are carried out with the empire specific level density formulation.

The slopes of the measured neutron spectra are well reproduced by the PACE code but not by the EMPIRE code. The double differential yield is better reproduced by the EMPIRE code and particularly so at the backward angles while the results obtained from the PACE code always over predicts it. The experimental double differential yield increases by 2 to 4 times when the projectile energy is increased from 110 MeV to 145 MeV. The angular distribution of the energy integrated yield obtained from the present experiment shows an enhanced emission in the forward angles compared to the results from the EMPIRE code and the experimental results from 110 MeV projectiles, but is lower than that given by the PACE code. It appears that the emission from 145 MeV  $^{19}\text{F}$  projectiles incident on a thick Al target may have some contribution from the pre-equilibrium emissions. Further investigations with varying projectile energies may help elucidate the picture.

## References

- [1] H.W. Patterson, R.H. Thomas, *Accelerator Health Physics*, Academic Press, New York, 1972.
- [2] ICRP Publication 74, *Annals of the ICRP*, 26 (3/4), 1996.
- [3] P.J. Taddei, J.D. Fontenot, Y. Zheng, D. Mirkovic, A.K. Lee, U. Titt, W.D. Newhauser, *Physics in Medicine and Biology* 53 (2008) 2131.
- [4] F. Wissmann, U. Giesen, D. Schardt, G. Martino, C. Sunil, *Radiation Environmental Biophysics* 49 (2010) 331.
- [5] P.K. Sarkar, T. Bandyopadhyay, G. Muthukrishnan, S. Ghosh, *Physical Review C* 43 (1991) 1855.
- [6] C. Sunil, A. Saxena, R.K. Choudhury, L.M. Pant, *Nuclear Instruments and Methods in Physics Research A* 534 (2004) 518.
- [7] C. Sunil, Nandy Maitreyee, P.K. Sarkar, *Physical Review C* 78 (2008) 064607.
- [8] M. Nandy, T. Bandyopadhyay, P.K. Sarkar, *Physical Review C* 63 (2001) 034610.
- [9] E.L. Hubbard, R.M. Main, R.V. Pyle, *Physical Review* 118 (1960) 507.
- [10] K. Shin, K. Miyahara, E. Tanabe, Y. Uwamino, *Nuclear Science and Engineering* 120 (1995) 40.
- [11] Gavron, *Physical Review C* 21 (1980) 230.
- [12] M. Herman, R. Capote, B.V. Carlson, P. Oblozinsky, M. Sin, A. Trkov, H. Wienke, V. Zerkin, *Nuclear Data Sheets* 108 (2007) 2655.
- [13] (<http://www.srim.org/>), (accessed 11.03.13).
- [14] A. Pantaleo, L. Fiore, G. Guarino, V. Patricchio, G. D'Erasmus, E.M. Fiore, N. Colonna, *Nuclear Instruments and Methods in Physics Research Section A* 291 (1990) 570.
- [15] T. Kurosawa, N. Nakao, T. Nakamura, H. Iwase, H. Sato, Y. Uwamino, A. Fukumura, *Physical Review C* 62 (2000) 044615.
- [16] R. Bass, *Physical Review Letters* 39 (1977) 265.